ACS NANO

www.acsnano.org

ARTICLE

Ultimate Spin Currents in Commercial Chemical Vapor Deposited Graphene

J. Panda,[§] M. Ramu,[§] Olof Karis, Tapati Sarkar, and M. Venkata Kamalakar*

Cite This: *ACS Nano* 2020, 14, 12771−12780

Read Online

ACCESS | Metrics & More | Article Recommendations | Supporting Information

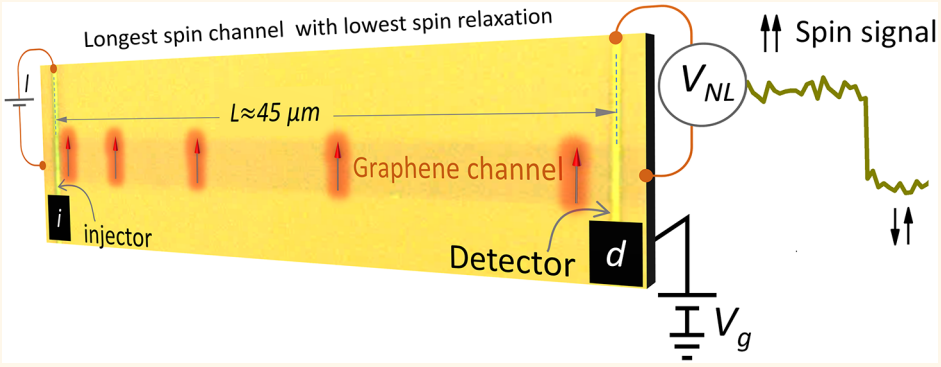

ABSTRACT: **Establishing ultimate spin current efficiency in graphene over industry-standard substrates can facilitate research and development exploration of spin current functions and spin sensing. At the same time, it can resolve core issues in spin relaxation physics while addressing the skepticism of graphene's practicality for planar spintronic applications. In this work, we reveal an exceptionally long spin communication capability of 45 μm and highest to date spin diffusion length of 13.6 μm in graphene on SiO_2/Si at room temperature. Employing commercial chemical vapor deposited (CVD) graphene, we show how contact-induced surface charge transfer doping and device doping contributions, as well as spin relaxation, can be quenched in extremely long spin channels and thereby enable unexpectedly long spin diffusion lengths in polycrystalline CVD graphene. Extensive experiments show enhanced spin transport and precession in multiple longest channels (36 and 45 μm) that reveal the highest spin lifetime of ∼2.5−3.5 ns in graphene over SiO_2/Si, even under ambient conditions. Such performance, made possible due to our devices approaching the intrinsic spin−orbit coupling of ∼20 μeV in graphene, reveals the role of the D'yakonov−Perel' spin relaxation mechanism in graphene channels as well as contact regions. Our record demonstration, fresh device engineering, and spin relaxation insights unlock the ultimate spin current capabilities of graphene on SiO_2/Si, while the robust high performance of commercial CVD graphene can proliferate research and development of innovative spin sensors and spin computing circuits.**

KEYWORDS: *graphene spintronics, spintronics, spin current, surface charge transfer doping, CVD graphene*

Spin current communication is the keystone to exploring spin current functions, realizing planar spin current applications, potential spin integrated circuits, and spin processors. So far, graphene is the only material that is practical for efficient spin transport,[1−4] primarily due to its inert[5] nature to the spin of electrons, and favorably high carrier mobility.[6] Efficient spin devices using large-scale graphene on industrial standard SiO_2/Si substrates are the way to go beyond basic spin transport experiments and realize graphene functional spintronic applications. Moreover, the exceptional mechanical resilience of graphene offers a fresh avenue for flexible graphene spintronics.[7] For more than a decade, research in graphene spintronics has shown several advancements, with some top reports displaying a spin diffusion length of ∼10 μm, in the single-crystalline exfoliated graphene built on atomically flat hexagonal boron nitride (hBN) substrates.[6,8,9] On the other hand, spin transport in large-scale chemical vapor deposited (CVD) graphene has also been demonstrated[3,10,11] and presents scope for scalability and industrial applications.

Received: April 22, 2020
Accepted: September 18, 2020
Published: September 18, 2020

https://dx.doi.org/10.1021/acsnano.0c03376
ACS Nano 2020, 14, 12771−12780

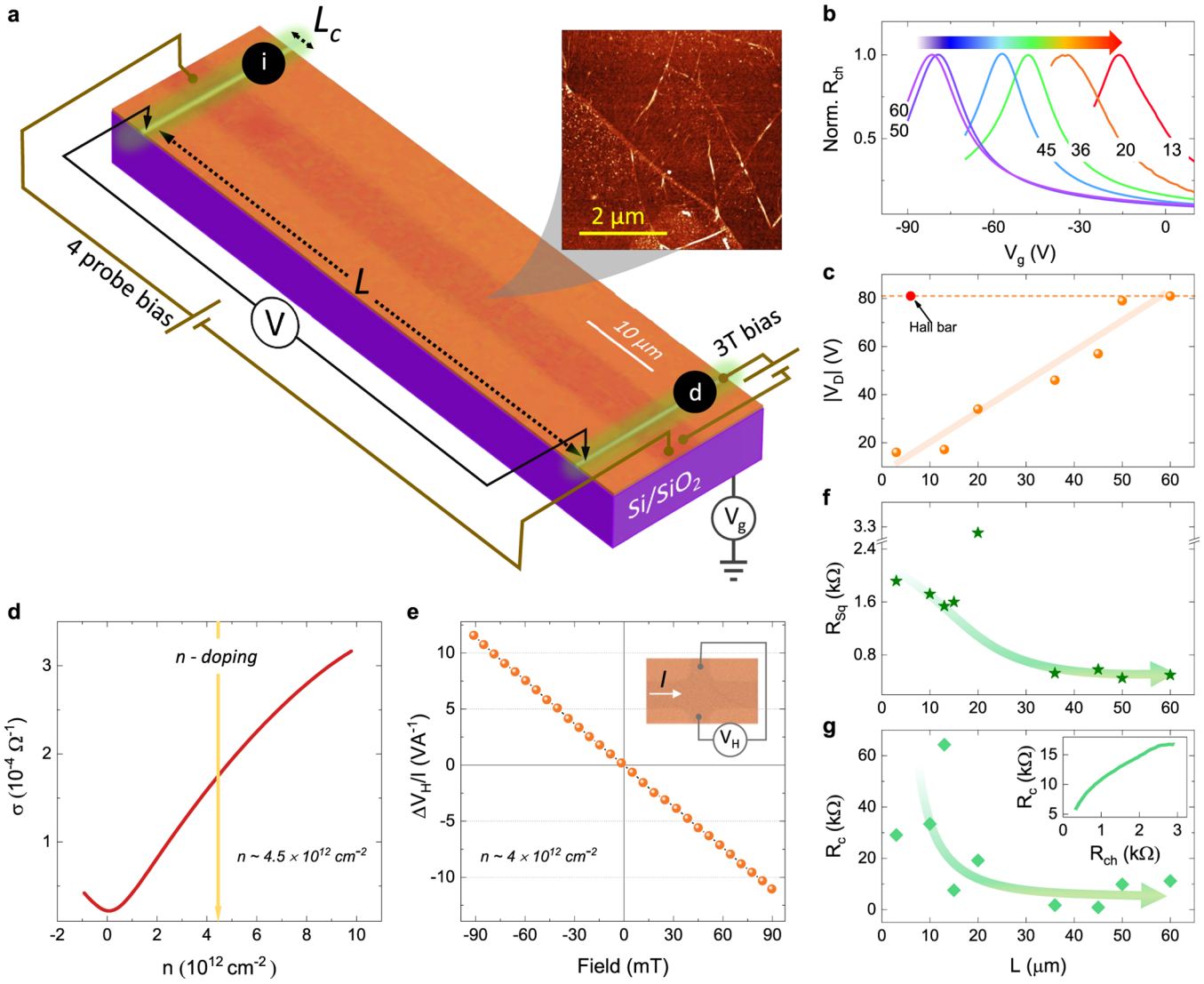

Figure 1. Electrical properties of long channel graphene spin devices. (a) Scheme with optical image of a CVD graphene channel of length $L \approx 60$ μm on SiO_2/Si with Co/TiO_x ferromagnetic tunnel injector i and detector d contacts of different widths. AFM image over a 5 μm × 5 μm area shows imperfections and the grainy nature of the commercial graphene. The circuit diagrams represent four-probe channel resistance and 3T contact resistance measurement configurations. (b) Normalized Dirac curves (channel resistance *versus* back gate voltage) measured in four-probe configuration for different channel lengths represented by the numbers (length in μm). (c) Dirac point (V_D) for different channel lengths. The reference V_D (red dot) corresponds to the measurement performed on a Hall bar with normal Ti/Au electrodes. The 3 and 13 μm channel devices are prepared on a single graphene sheet. (d) Conductivity of the graphene channel as a function of carrier concentration shows initial high doping of the H-bar sample. (e) Change in Hall voltage as a function of an out-of-plane magnetic field. Inset: Optical image of the cross-arm for Hall mobility measurement. (f) Square resistance (R_{sq}) of graphene measured in the four-probe configuration for different channel lengths. (g) Three terminal equivalent contact resistance $R_c = \frac{2R_iR_d}{R_i+R_d}$ (where R_i and R_d are the injector and detector resistances, respectively) for different channel length devices. Inset: Variation of R_c *vs* R_{ch} for a single graphene device. The arrows represent a guide to the eye.

Understandably though, in this form of polycrystalline graphene, the grain boundaries, intrinsic defects, and accumulated impurities during fabrication have limited spin diffusion lengths to ∼2−6 μm at room temperature,[3,10,11] leading to uncertainties about its ultimate utility. Recently, spin diffusion lengths λ of ∼7−9 μm and spin lifetimes τ of ∼2−3 ns were reported in special CVD graphene grown over a Pt substrate.[12] This performance is higher than the previously obtained best values in CVD graphene grown on Cu substrates.[3] It has been reported that a platinum substrate facilitates high-temperature (1100 °C) nucleation and crystallization, resulting in millimeter-sized CVD graphene crystals.[13] Large single-crystalline domains could eliminate grain-boundary defects and scattering that could lead to higher spin lifetimes in the nanosecond regime, as observed in high-quality exfoliated graphene heterostructures[6,8,9] or single-crystalline CVD graphene[14] devices. Unlike such single crystals, commercially obtained CVD graphene grown over Cu is polycrystalline and characterized by realistic structural flaws, with a grain size of ∼100 nm to 5 μm, and added ripples and defects caused during the fabrication steps[15] that limit its electronic quality. The skepticism over CVD graphene's spintronic performance is well placed because, even today, typical values of the spin diffusion length in polycrystalline

https://dx.doi.org/10.1021/acsnano.0c03376
ACS Nano 2020, 14, 12771−12780

CVD graphene is limited to λ ~1.5−2.5 μm at room temperature.[16] Presently, nearly a dozen companies provide commercial graphene on SiO_2/Si of up to 6 in. wafer size. Regardless of the cost issues of the Pt substrate-based growth,[13] for graphene spintronic devices to be of high relevance for industrial applications, it is essential to obtain high performance in commercial polycrystalline graphene grown over Cu. Very recently, theoretical results suggested the independence of λ on the grain size in polycrystalline graphene.[17] However, there has been no matching experimental demonstrations of this work that can verify high λ in polycrystalline graphene, and obtaining maximum performance out of commercially available CVD graphene remains a challenge.

In this work, we demonstrate a record-high performance in commercial CVD graphene by investigating multiple long-distance devices fabricated on standard SiO_2/Si substrates. Our experiments reveal the longest spin communication capability of 45 μm in graphene spintronics, with the highest to date spin parameters observed for any form of graphene on SiO_2/Si substrates. Probing extremely long channel lengths in spin devices in the range up to 60 μm, here we reveal a clear connection of channel length on doping and active spin relaxation in graphene, establishing the fact that polycrystallinity is not a hurdle to obtaining maximum performance.

RESULTS AND DISCUSSION

For fabricating the graphene spin devices, we employed commercially obtained CVD graphene over a 4 in. Si wafer with a SiO_2 oxide layer thickness of ~285 nm that showed initial high n-type doping. The single-layer nature of such graphene has been confirmed using Raman spectroscopy (see Supporting Information, Figure S1). First, the CVD graphene on a SiO_2/Si wafer was patterned using photolithography into several 33−85 μm long stripes. On these patterned CVD graphene islands, ferromagnetic tunnel contacts (Co/TiO_x) consisting of a layered structure of TiO_x (0.8 nm)|Co (60 nm)|Al (5 nm)|Au (5 nm), with interelectrode spacing in the range of 3−60 μm, were fabricated by e-beam lithography and e-beam evaporation, involving an oxidation process of the initial Ti layer (as elaborated in Methods). In Figure 1a, an optical microscope image of a spin device along with electrical characterization schemes is displayed.

Contact-Induced Surface Charge Transfer Doping and Device Doping in Graphene Spin Devices. The quality of the graphene channel and contacts is crucial for establishing efficient spin transport in graphene. It is usually observed that once a clear spin transport is established with contacts overcoming the conductivity mismatch criteria,[18,19] electrostatic doping appreciably enhances spin transport in graphene.[3,8] This makes it interesting to see how inherent device doping controls spin transport. In particular, contacts can lead to surface charge transfer doping (SCTD), which could significantly shift the Dirac point (V_D).[20−23] Furthermore, there is an ambiguity on how the spin injection−detection contact separation or the channel length L influences the spin parameters. Fabricating devices with very long channels (as shown in Figure 1a) allows us to carefully probe the impact of SCTD and contact separation in graphene spin devices and their effects on performance and spin relaxation, and ultimate spin device engineering. To investigate that, first, we performed gate voltage V_g-dependent electrical measurements of channel resistance R_{ch} in four probe configurations to obtain the Dirac point (V_D) for devices with different channel lengths L. A clear dependence of V_D on device L is displayed in Figure 1b, with results in Figure 1c showing a huge change in V_D by nearly 60 V ~10^{13} cm^{-2} (change in carrier concentration n). We observed that at V_g = 0, the as-prepared devices showed a high doping of n ~ 10^{12} cm^{-2} (as shown in Figure 1d for a Hall-bar sample). We also performed Hall measurements with nonmagnetic contact (Ti|Au) that revealed similar carrier concentration (Figure 1e) and a $V_D \approx -80$ V (red dot in Figure 1c), similar to devices having the longest L. The systematic shift in V_D with L shown in Figure 1c indicates that the Co contacts with a 0.8 nm TiO_x barrier layer in our devices contribute to p-type doping. Such doping can lead to channel length-dependent sheet resistance and contact resistance in graphene spin devices. In Figure 1f, we show the sheet resistance of monolayer graphene in the range 560−2000 Ω/sq, fairly varying with the channel length, except for 3300 Ω/sq for the 20 μm channel. The observed length dependence of the electrical parameters can be inferred as the fading contribution of contact-induced SCTD with increased channel length. The SCTD is confined to contact vicinity (as portrayed in Figure 1a by the effective contact region L_C) with its doping profile decaying within a region of length ~200−300 nm to the equilibrium carrier concentration in graphene, as demonstrated by scanning photocurrent experiments.[24] While measuring the Dirac curves by the four-probe method, the contribution due to SCTD to the channel resistance is additive. Hence, for a channel $L \gg L_C$, such contribution is minimum, which is consistent with our observations here. Note that device-to-device variations can also occur in graphene spin devices. However, wafer-scale graphene from the same batch has considerably uniform doping.[3] For devices prepared under the same fabrication route, we observed reasonably good mobility μ of ~2000−3000 cm^2 V^{-1} s^{-1} in the majority of the devices presented in Figure 1 (except for the 20 μm long channel device) and uniform electrical properties in single sheets of graphene (see Supporting Information, Figure S2). Despite some deviations, the general trends of device parameters in Figure 1 show high consistency. To achieve homogeneity in the doping profile in the channel,[25] we avoided multiple contacts within the long channels. On the other hand, measurement on devices with multiple contacts on single graphene sheets also showed an L-dependent shift in V_D and a clear impact of contacts in sheet resistance, with up to ~25% enhanced R_{sq} in short channels (summarized in Figure S3 of the Supporting Information), which qualitatively agree with the observations presented in Figure 1. We do not rule out the contributions due to process-related device doping that could depend upon device structure and dimensions, which could also influence extrinsic doping levels in graphene. Nevertheless, our systematic dependencies are consistent with SCTD-induced variations in graphene devices[22,23] and suggest that the equilibrium doping concentration is guided by the longest continuous channel L (without intermediate contacts) in a particular device (Figure S3 of the Supporting Information). The contact resistances in our devices were measured in the standard three-terminal 3T bias configuration shown in Figure 1a. Typical values of $R_c = \frac{2R_iR_d}{R_i + R_d}$ (where R_i and R_d are the injector and detector resistances, respectively) were found to vary in the range ~1−70 kΩ with channel length L, as shown in Figure 1g. Such contacts show tunneling IV characteristics (see Supporting

https://dx.doi.org/10.1021/acsnano.0c03376
ACS Nano 2020, 14, 12771−12780

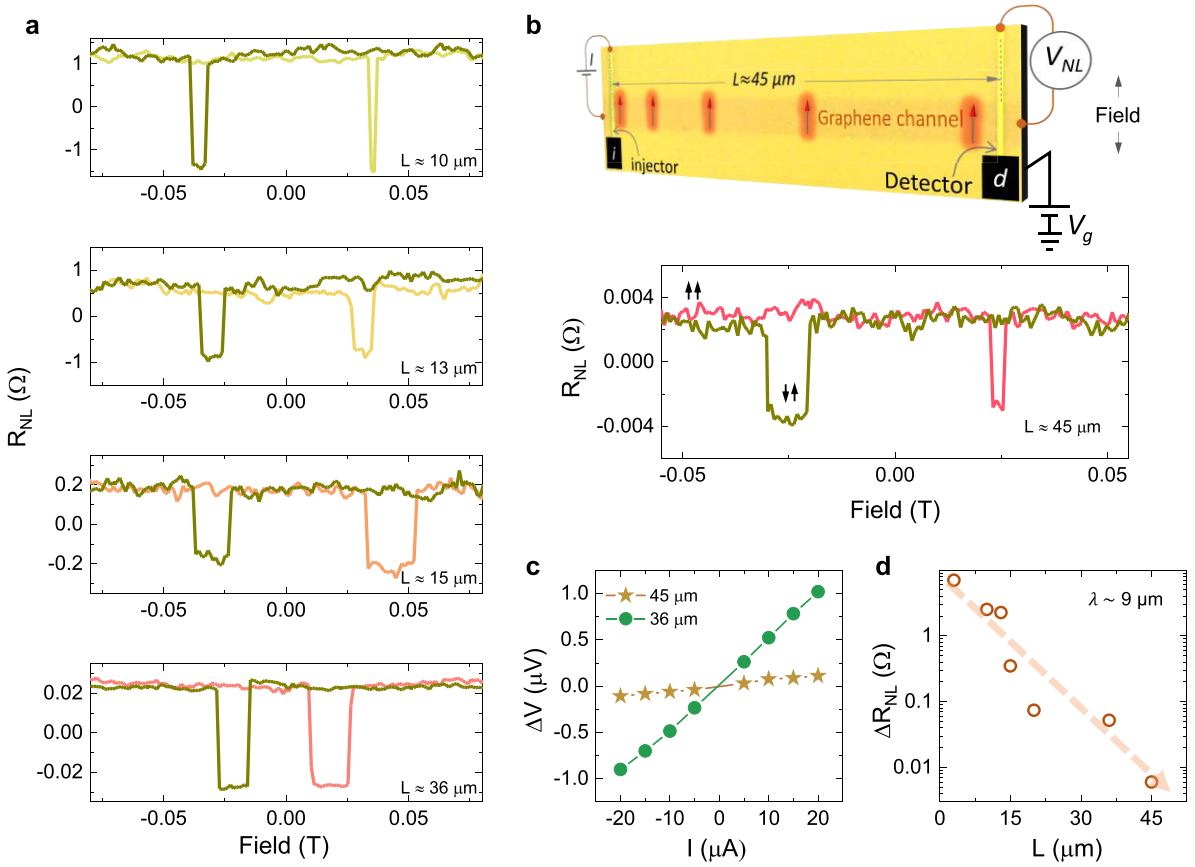

Figure 2. Spin transport in long channel graphene spin devices. (a) Nonlocal spin-valve signal for different channel lengths with applied in-plane magnetic field ($B_{\|}$) sweep from $-B$ to $+B$. (b) Optical image of a CVD graphene spin device with a channel length of $L \approx 45$ μm along with room-temperature spin signal obtained in the device. The high and low values of NL resistance R_{NL} correspond to the parallel (↑↑ or ↓↓) and antiparallel (↑↓ or ↓↑) configurations of the ferromagnetic injector and detector electrodes, respectively. (c) Bias-dependent nonlocal spin valve signal (ΔV) for channel lengths of 36 and 45 μm. (d) ΔR_{NL} ($\Delta V/I$) as a function of channel length L following an exponential decay, $\Delta R_{NL} \approx e^{-L/\lambda}$.

Information, Figure S4) and bypass the conductivity mismatch problem.[18,19] Despite fluctuations, the overall decreasing trend in Figure 1g shows that increased sheet resistance leads to enhanced interface resistance in all our devices. This can be further confirmed by the 3T contact resistance *vs* channel resistance measured in a single device by gate sweeping, shown in the inset of Figure 1g. The similar response of the tunnel contact resistance R_c to the graphene sheet resistance R_{sq} is expected from the theory of tunneling, where the conductance is proportional to the product of the density of states of contact and graphene, and suggests a well-preserved graphene below the tunnel barrier. Overall, our results offer new insights into how the contributions due to SCTD and device doping can be quenched in long channels, leading to channel and contact resistance engineering by device dimensions. Consequently, channel length/contact separation L can influence doping contributions and can serve as a key parameter to engineer-control spin devices with specific channel and contact resistances, hence spin accumulation and polarization in graphene spin devices. Such an explicit control has not been reported earlier in graphene spin devices.

To Date Longest Spin Communication with Highest Performance. For spin transport measurements, here we focused on long channel devices ($L \geq 10$ μm). Usually, realizing long channel devices makes it more challenging to observe spin transport, as the spin diffusion profile decays exponentially with the increasing channel length, and the spin signal is obscured by the electrical noise, making experimental observations possible only for high-quality devices. Here, we performed comprehensive nonlocal spin transport measurements on several devices with extremely long channels to uncover the reliability of the commercial CVD graphene platform. For these measurements, the nonlocal concept of spin injection and detection is a precision method to establish pure spin current transport. In Figure 2a and b, we present the spin-valve measurements performed on devices with different channel lengths L. As illustrated in the spin transport scheme in Figure 2b, spin current injection into graphene is performed by an electric current passing through a ferromagnetic injector (i)−graphene circuit, while an isolated detector (d)−graphene circuit measures the spin accumulation in graphene. The difference in such voltage for parallel (↑↑ or ↓↓) and antiparallel (↑↓ or ↓↑) configurations of injector and detector provides a direct measure of the spin transport through graphene. This signal is obtained by the spin-valve measurement technique, where an in-plane magnetic field ($B_{\|}$) is swept along the easy axis of the ferromagnetic electrodes. Due to the difference in the coercive fields of the injector and detector electrodes, the relative magnetic orientations of the spin injector and spin detector ferromagnetic electrodes are switched from parallel to antiparallel configuration. The corresponding nonlocal spin voltage, estimated as ΔV (ΔV_{NL}

https://dx.doi.org/10.1021/acsnano.0c03376
ACS Nano 2020, 14, 12771−12780

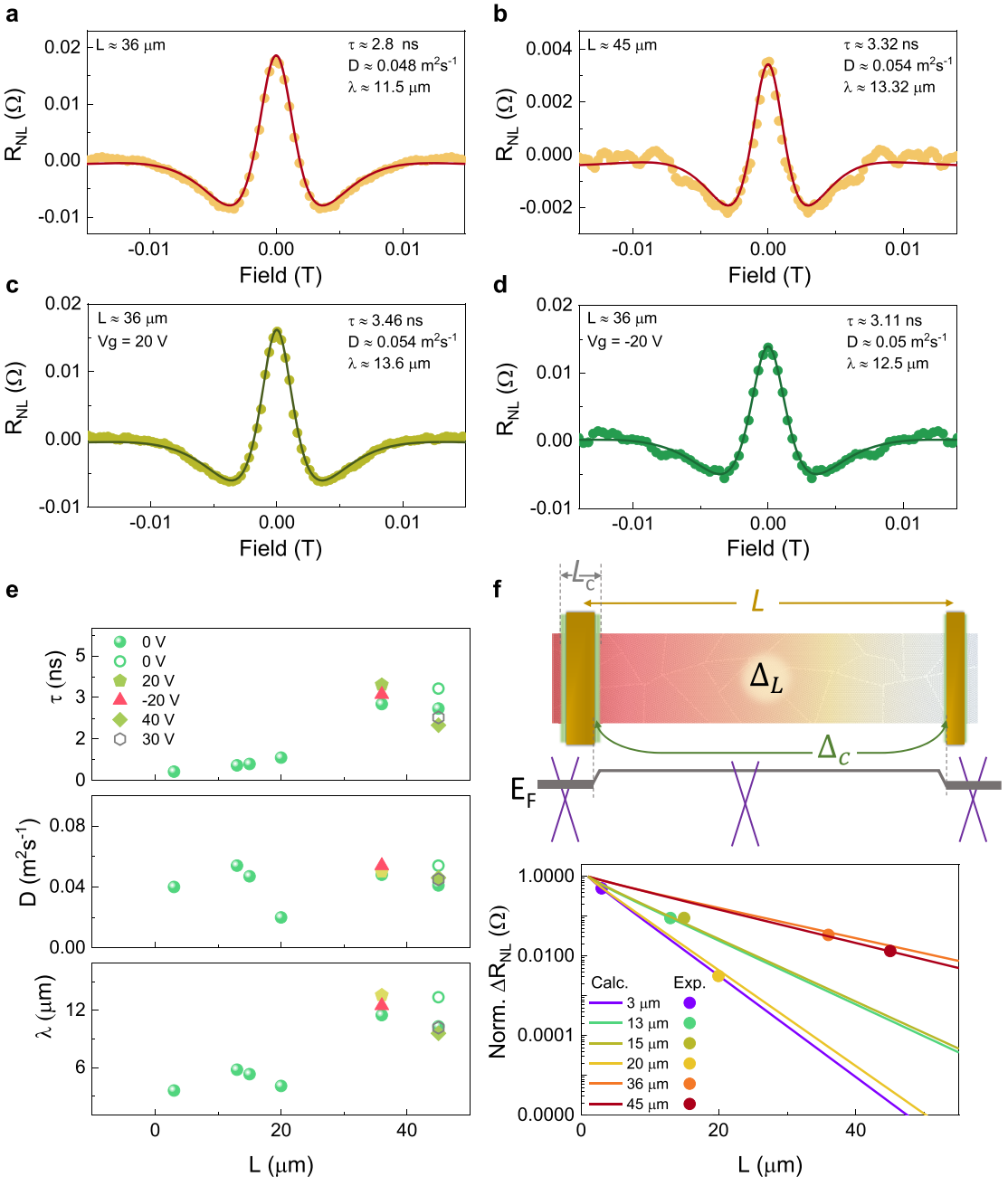

Figure 3. Spin precession in long channel graphene spin devices. (a) Hanle signal for a channel length of $L \approx 36$ μm. (b) Hanle signal for a channel length of $L \approx 45$ μm. (c), (d) Hanle signals for a channel length of $L \approx 36$ μm at $V_g = 20$ V and $V_g = -20$ V, respectively. (e) Spin lifetime τ, spin diffusion constant D, and spin diffusion length λ as a function of channel length L. The open green circle for $L \approx 45$ μm (presented in (b)) is a data set measured after nearly 10 months, compared to initial measurement values represented by the solid symbols. (f) Plots of calculated ΔR_{NL} (normalized with respect to calculated ΔR_{NL} at $L = 0$ for each device) as a function of channel length, with experimental points taken from spin-valve amplitudes; the top scheme represents spin diffusion in a graphene device (presented by the faded red color) with a doping profile across the device. Δ_C and Δ_L represent the spin−orbit coupling in the contact regions and channel, respectively.

$= V_{NL}(\uparrow\uparrow) - V_{NL}(\uparrow\downarrow)$), gives rise to nonlocal resistance $\Delta R_{NL} = \Delta V/I$. As presented in Figure 2a and b, we could realize high-performance spin transport in several long channels $L \geq 10$ μm, which includes extremely long channels of 36 and 45 μm at room temperature. Spin communication up to such lengths has never been reported in graphene spin valves, neither for exfoliated nor CVD forms. The spin communication capability, *i.e.*, the experimentally demonstrated distance over which spin currents can propagate, is nearly 300% longer compared to the spin communication achieved with the highest spin parameters in commercial CVD graphene[3] and significantly higher than the state-of-the-art reports using a Pt-based CVD graphene system.[12]

A linear dependence of the spin signal with bias current is observed in the devices (Figure 2c), implying a stable bias-independent polarization for currents employed here for electrical spin injection. We consistently observed spin transport in several long-distance devices with channel lengths

https://dx.doi.org/10.1021/acsnano.0c03376
ACS Nano 2020, 14, 12771−12780

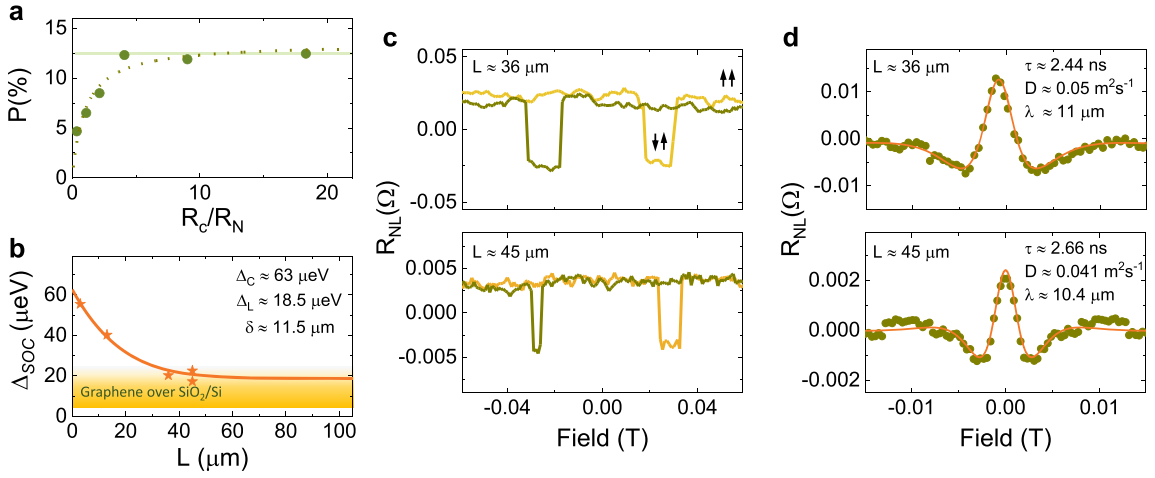

Figure 4. (a) Polarization *versus* R_c/R_N. The dotted line is a fit of $P \sim \frac{R_c}{R_N}/\left(1+\frac{R_c}{R_N}\right)$ following Fert–Jaffrès calculations.[19] (b) Spin–orbit coupling values calculated from observed spin diffusion lengths from high-performance devices ($\mu \approx 2000-3000$ cm^2 s^{-1} V^{-1}) and devices without intermediate contacts. (c) Spin-valve and (d) Hanle spin signals obtained under ambient conditions for 36 and 45 μm long channel devices.

of L ~10, 13, 15, 20, 36, and 45 μm (summarized in Figure S5). The length dependence of spin signal ΔR_{NL} presented in Figure 2d obtained from different devices shows some fluctuations from exponential decay, which can be attributed to the fact that different devices have different doping and interface resistance R_c, and hence dissimilar spin polarizations. Nevertheless, even a rudimentary exponential dependence of the form $e^{-L/\lambda}$ yields a very high value of spin diffusion length ($\lambda \approx 9$ μm), which is the highest value for commercial graphene and very high, even when compared to the best reports in top-quality exfoliated graphene heterostructures at room temperature,[6,8] realized here in an industrial-grade system. Furthermore, the enhanced device quality can be assessed from the fact that the nonlocal spin resistance for $L \approx 36$ μm is up to one order higher than earlier reports in commercial graphene[3,11] obtained in channel lengths that are 10–20 μm shorter.

In addition to spin-valve measurements, spin precession measurements not only confirm spin transport in graphene but allow for the determination of spin parameters such as spin diffusion length λ and spin lifetime τ. For this, we performed Hanle measurements, where spin currents through graphene channel undergoing spin precession with a Larmor precession frequency $\omega_L = \frac{g\mu_B}{\hbar}B_\perp$ (g, μ_B, and $\hbar$ are standard constants), about an out-of-plane magnetic field ($B_\perp$), result in the variation in the nonlocal voltage V_{NL} for parallel (↑↑) and antiparallel (↑↓) configurations of the injector and detector. The precession of diffusion spin current (with a spin diffusion constant D) is accompanied by spin relaxation in channel L with spin lifetime τ, and the emerging Hanle signal follows the analytical solution[26] to the steady-state Bloch diffusion eq 1

$$D\nabla^2\mu_s - \frac{\mu_s}{\tau} + \omega \times \mu_s = 0 \tag{1}$$

where $\mu_s = \mu_\uparrow - \mu_\downarrow$ is the net spin polarization vector with the direction pointing to the polarization axis. The Hanle spin signal is analyzed using the analytical solution[26] of eq 1, given by eq 2:

$$R_{NL}^{\uparrow\uparrow \text{or} \downarrow\uparrow} = Re\left(\pm\frac{2P^2R_N}{\sqrt{1+i\omega\tau}}\frac{e^{-L/\sqrt{D\tau/(1+i\omega\tau)}}}{\left(\frac{R_N}{R_i\sqrt{1+i\omega\tau}}+2\right)\left(\frac{R_N}{R_d\sqrt{1+i\omega\tau}}+2\right)-e^{-2L/\sqrt{D\tau/(1+i\omega\tau)}}}\right) \tag{2}$$

where $R_N = \frac{R_{ch}\lambda}{L}$ is the spin resistance of the channel and R_i and R_d represent the injector and detector resistances, respectively. Fitting the Hanle spin signals measured from both ↑↑ and ↓↑ configurations, together as $R_{NL}=\frac{R_{NL}^{\uparrow\uparrow}-R_{NL}^{\downarrow\uparrow}}{2}$, we obtain the spin parameters D and τ, and the spin diffusion length $\lambda = \sqrt{D\tau}$. Such spin precession signals for the devices with $L \approx 36$ μm and $L \approx 45$ μm along with the fittings are shown in Figure 3a and b, respectively. Fitting R_{NL} for $L \approx 36$ μm yields $\tau \approx 2.8$ ns and $D \approx 0.048$ m^2 s^{-1}, resulting in a spin diffusion length of $\lambda \approx 11.5$ μm. In Figure 3b, for the device with the longest channel length $L \approx 45$ μm, we observed a maximum $\lambda \approx 13.3$ μm with a high spin lifetime of $\tau \approx 3.3$ ns.

These spin diffusion lengths are the highest values achieved so far, not only for CVD graphene but in general, for graphene spin devices on standard large-scale substrates. Usually, it is observed that electrostatically enhanced carrier densities (applying a high gate voltage of ~80 V) lead to higher performance in spin lifetimes in single-crystalline encapsulated samples. In contrast, here, high values are obtained on standard commercial CVD graphene on SiO_2/Si without the application of any gate voltage. The application of the gate voltage led to further enhanced values, as shown in Figure 3c and d for $L \approx 36$ μm, with $\lambda \approx 13.6$ μm, $\tau \approx 3.5$ ns at $V_g = 20$ V and $\lambda \approx 12.5$ μm, $\tau \approx 3.1$ ns at $V_g = -20$ V. As shown in Figure 3e, for the as-prepared device with $L \approx 45$ μm, we obtained $\lambda \approx 10.4$ μm

https://dx.doi.org/10.1021/acsnano.0c03376
ACS Nano 2020, 14, 12771–12780

(green dot), independent of the gate voltages within a similar range. We observe a reasonable agreement between D and the charge diffusion coefficient $D_c \approx 0.025-0.038$ m^2 s^{-1} evaluated from electrical measurements, which confirms the reliability of the Hanle fitting procedure.[27−29]

In Figure 3e, we show how the spin parameters evolve with the channel length, showing hugely enhanced spin metrics τ and λ for longest channels $L \approx 36$ μm and $L \approx 45$ μm, compared to relatively high values in shorter channels having similar D. For extremely long channels $L \approx 36$ μm ($\mu \approx 2700$ cm^2 s^{-1} V^{-1}) and $L \approx 45$ μm ($\mu \approx 2200$ cm^2 s^{-1} V^{-1}), the spin lifetime approaches values of ∼3.5 ns. It is also worth noting that for $L \approx 20$ μm ($R_{sq} \approx 3300$ Ω, $\mu \approx 1500$ cm^2 s^{-1} V^{-1}), the spin lifetime is higher than shorter channels having mobility $\mu \approx 2700$ cm^2 s^{-1} V^{-1}. These observations suggest the role of contacts in enhanced spin relaxation in shorter channel length devices. Also, our device dimensions are higher than the maximum spin diffusion length,[30] which ensures proper evaluation of the spin metrics. Furthermore, as shown in Figure 3f, the calculated spin-valve signals with the obtained spin parameters match our experimental spin-valve amplitudes, further validating the spin parameters. Since the doping and interface conditions are distinct for different channel lengths, we have evaluated the polarization and contact resistance. In Figure 4a, we show the systematic enhancement of the spin polarization P guided by the ratio of contact resistance R_c and channel spin resistance R_N, revealing a high steady polarization $P \approx 12.5\%$, highest for TiO_x barriers in graphene spin devices. It indicates that with our fabrication process, contacts with high P can be reproducibly made in CVD graphene by engineering devices with high values of R_C/R_N in accordance with Fert−Jaffrès theory.[19]

Spin Relaxation in Commercial Polycrystalline CVD Graphene. Large-scale polycrystalline graphene grown over Cu substrates features grain sizes on the order of a few hundred nanometers[31] to a few microns.[32] In the specific brand of commercial graphene that we employed here, direct observation of grain boundaries established grain size in the range of ∼2−10 μm, confirmed through multiple techniques.[33] Overall, studies suggest a median grain size of 3−4 μm as well as smaller submicron domains for graphene grown over Cu revealed by atomic resolution characterization.[31] Understanding spin relaxation in such a form of graphene allows for longer channels and can generate valuable insights about core spin relaxation in graphene. In graphene, the natural sources of spin relaxation are the Elliot−Yafet (EY) relaxation[34] and D'yakonov−Perel' (DP) mechanism,[35] which yield theoretical values of τ_s in the μs range.[5,34,36] Earlier experimental studies of spin transport in graphene considered the quantitative effects of EY[37] or both kinds of mechanisms to explain the observations,[2,3,38] although $\tau \approx 0.5-1$ ns were obtained in such experiments. In principle, for experimentally observed lifetimes, corrugations and flexural distortions,[39] ripples, or wrinkles[39,40] featured in CVD graphene are known to have less impact on spin relaxation. Beyond the EY and DP mechanisms, other finer mechanisms such as spin−pseudospin entanglement in the quasi-ballistic transport regime[41,42] and magnetic moments, vacancies, and defects at grain boundaries[43,44] in the diffusive transport regime in polycrystalline graphene could lead to experimentally observed spin lifetimes of about a few hundred ps. Consequently, imperfections in commercial CVD graphene should contribute substantially to spin relaxation, which remained a key motivation behind aiming for high performance in single-crystalline graphene (both for CVD and exfoliated graphene) so far. However, recent theoretical calculations performed on polycrystalline graphene show that spin relaxation is independent of average grain size, which should not affect the upper limit of spin transport in CVD graphene.[17] When the DP mechanism is the natural dominant spin relaxation mechanism, spin−orbit coupling (Δ_{SOC}) can lead to spin diffusion length $\lambda \approx \frac{V_F \hbar}{2\sqrt{2}\Delta_{SOC}}$, where V_F is the Fermi velocity.[17,45,46] In our high electronic quality spin devices, we observe $\frac{\tau_{EY}}{\tau_{DP}} \approx \left(\frac{2\tau_p E_F}{\hbar}\right)^2 \gg 1$, signifying that DP is the dominant spin relaxation mechanism. In the longest spin communication channels of 36 and 45 μm, we observed spin diffusion of $\lambda \approx 13.5$ μm, which translate to $\Delta_{SOC} \approx 17$ μeV, a value expected for graphene on inert substrates such as SiO_2/Si. Obtaining the experimentally lowest Δ_{SOC}, intrinsic to graphene, suggests that we have reached the maximum spin diffusion length in graphene over the industry-standard SiO_2/Si substrate. This is an important finding that has been possible here only due to the highest quality spin transport achieved over extremely long spin channels. In addition, this insight also resolves the existing ambiguity about channel length dependence of spin transport parameters in graphene,[3,12] revealing how device dimensions can alter doping, device properties, and the dominant spin relaxation at contacts for shorter channels. In general, the spin relaxation in graphene near the contact region L_C could originate from either EY or DP mechanism. While spin absorption[28,38,47] could affect spin lifetime, to account for that, we implemented contact resistances of injector and detector into the Hanle fitting analysis. Due to the high-quality tunnel barrier fabrication, as evidenced by the highest spin polarization $P \approx 12.5\%$ in CVD devices with TiO_x barriers, the relatively low shift in V_D in a single sheet of graphene with higher mobility (see Supporting Information, Figure S3), and faithful gate-dependent interface resistance (Supporting Information, Figure S6), graphene can be considered to be structurally preserved under the contacts. Therefore, we assume the dominant relaxation under the contacts also to be the DP mechanism due to Rashba spin−orbit coupling. In Figure 4b, we plot the dependence of the resultant Δ_{SOC} as a function of channel length L in high electronic quality spin devices. To deconvolute the Rashba SOC below the contacts and the SOC in the channel, we apply an empirical function (eq 3) consisting of Δ_C and Δ_L representing the SOC in contacts and channel, respectively, and a characteristic length δ quantifying the decay of contact contribution *versus* dominance of channel contribution. Note that here we chose to plot the highest performance devices and channels without additional contacts to rule out local inhomogeneities.[25]

$$\Delta_{SOC} = \sqrt{\Delta_C^2 e^{-L/\delta} + \Delta_L^2 (1 - e^{-L/\delta})} \quad (3)$$

Fitting the data in Figure 4b with eq 3 yields $\Delta_L \approx 18.5$ μeV, $\Delta_C \approx 63$ μeV, and $\delta \approx 11.5$ μm, suggesting that for very long channel lengths $L \gg \delta$, the spin relaxation is dominated in the channels, compared to much shorter channel devices of $L \ll \delta$, where contact relaxation is significant. In the intermediate regime, as for $L \approx 13$ μm, we still observe considerable contribution from the contacts causing the relatively lower value of τ, despite having similar spin diffusion constant D. The contact $\Delta_C \approx 63$ μeV is a reasonable value considering that the

https://dx.doi.org/10.1021/acsnano.0c03376
ACS Nano 2020, 14, 12771−12780

contact region could lead to an effective Rashba SOC higher than the SOC in the channel region. From these values, the ratio of contact to channel spin relaxation rates $(1/\tau) \sim \left(\frac{\Delta_C}{\Delta_L}\right)^2 \approx 12$, implying that relaxation near the contacts can be an order faster than inside the channel. For each device, we have nearly 600 nm of total contact width for an injector/detector ~250−350 nm pair. Considering a spread of ~100 nm in the contact SOC region and a total contact region of ~0.8−1 μm for an injector−detector set responsible for the relaxation near and under contacts, the one order higher characteristic length $\delta \approx 11.5$ μm appears reasonable. In simpler terms, in a device consisting of short contact regions connected by a longer channel region, the Δ_{SOC} is an effective spatial value that depends upon how much spins explore the different regions *via* diffusive transport, and the weight of their relative contributions evolves with L. Since the fundamental length for such a transport process is spin diffusion length λ, the characteristic length δ is expected to correspond to λ. This we observe as $\delta \approx 11.5$ μm matches well with λ obtained from both the spin-valve (~9 μm) and Hanle measurements (~10−13.6 μm). These assessments provide consistent support to our model. In graphene devices, other contact-induced dephasing effects[28,38,47] and proximity of reference contacts, if placed closer than spin diffusion length to the injection contact,[30] also contribute to contact-related spin relaxation. Material quality and device fabrication processes are vital for observing enhanced spin parameters. Achieving improved know-how in each step of fabrication, such as patterning graphene, deposition of contacts, and liftoff, leads to significant improvement in the final device quality. In particular, we have achieved two things here: (a) with our TiO_x barrier process of contacts, we could observe the highest attained value of 12.5% polarization for such barriers in multiple devices, which signifies the achieved quality of interfaces. Obtaining such a value in multiple devices with strikingly systematic dependence of P on R_c/R_N (Figure 4a) suggests that our barrier quality is reproducibly uniform. In addition to such barrier quality, (b) having a good quality channel with a mobility of ~2000−3000 $cm^2\ s^{-1}\ V^{-1}$ dramatically improves the feasibility of obtaining extremely long-distance spin transport. Enabling such devices leads to extremely long-distance spin communication, which we achieved here in the 36 and 45 μm channel length devices. This helps in reducing the contribution of contact-induced relaxation in graphene devices, leading to the extraction of the highest spin parameters in high-quality CVD graphene devices and understanding the inherent spin relaxation mechanism.

Robust Spin Transport under Ambient Conditions. Finally, to further probe the strength of our longest-channel devices, we performed measurements under ambient conditions of temperature and pressure. As shown in Figures 4c and d, the quality of spin transport is nearly unaffected under standard atmospheric conditions, revealing similar high λ values as observed in measurements under vacuum. These comprehensive measurements serve to address the existing skepticism by showing the highest performance in large-scale graphene in multiple long-distance channels and associate the observed performance with device properties and spin relaxation. A robust large-scale platform with high performance is not only necessary to create reliable means for innovative spin current functions but also research and development (R & D) exploration of graphene spintronics applications. Such potential applications could include employing graphene to redefine magnetoresistive position, angle, or velocity sensing or advanced beyond-CMOS spin-logic memory circuits, including the further development of flexible spin circuits.[7,48] In this context, our present work demonstrates extraordinary performance and provides fresh insight into efficient graphene spin device engineering with commercial CVD graphene. This is a significant step forward in taking graphene spintronics out of the few laboratories into industrial R & D. This work, in particular, also inspires the exploration of other two-dimensional CVD-grown materials,[49−52] multiple layered graphene heterostructures,[53] and employing industrially compatible processing methods[15,54] for advancing spintronic applications.

CONCLUSIONS

In conclusion, we have demonstrated exceptionally long spin communication in graphene up to 45 μm at room temperature, with the highest to date achieved spin diffusion length of 13.6 μm and spin lifetime of ~3.5 ns in graphene over industry-standard substrates. This performance, realized in commercial polycrystalline CVD graphene, is a colossal enhancement to existing state-of-the-art values of spin transport in graphene on SiO_2/Si and shows stable high-spin diffusion lengths, even under ambient conditions. We observe that graphene device channel length can impact surface charge transfer doping at contacts and device doping, leading to channel length-dependent spin metrics and spin relaxation. By realizing extremely long channel spin communication, we attained the lowest intrinsic spin−orbit coupling Δ_{SOC} ~20 μeV of graphene, leading to the observation of theoretically possible ultimate spin diffusion length, irrespective of the grain boundaries in polycrystalline graphene. Consequently, such devices made it possible to identify and quantify the DP spin relaxation in channels and contacts. Our comprehensive demonstration of high performance, with robustness and high-resolution understanding of spin relaxation, establishes the impact of commercial polycrystalline CVD graphene for spintronics while creating realistic R & D prospects for the exploration of innovative spin current functions and large-scale spin-computing circuits.

METHODS

Device Fabrication. Devices were prepared using commercially procured CVD graphene on Cu (Graphenea Inc.) transferred over a 4 in. SiO_2/Si wafer prepatterned with Au marks. The CVD graphene was first patterned into several 33−85 μm long stripes of 5 μm width by photolithography and 50 W oxygen plasma etching. The remaining photoresist was removed with acetone at 70 °C, followed by rinsing with isopropanol (IPA). Ferromagnetic tunnel contacts having different spacings (3−60 μm) were fabricated on graphene stripes by e-beam lithography patterning and metal liftoff. For the electrodes, an optimized layer of 0.8 nm evaporated titanium metal was first oxidized to form a tunnel barrier layer of TiO_x. Following this, e-beam-assisted metal evaporation was performed to deposit successive layers of 60 nm Co, 5 nm Al, and a top oxidation protection layer of 5 nm Au. Finally, liftoff was achieved in hot acetone, rinsed by IPA. The obtained devices feature contacts with widths in the range of 150−350 nm and active contact area with graphene of ~1 μm^2. The devices were imaged using an optical microscope, with the optical parameters adjusted to observe the contrast of graphene over SiO_2/Si.

Graphene Characterization. Raman spectroscopy was performed to confirm the single-layer quality of CVD graphene.

Electrical and Spin Transport Measurements. Electrical characterization and spin transport measurements were performed in a helium/nitrogen flow cryostat in high-vacuum condition (~10^{-7}

https://dx.doi.org/10.1021/acsnano.0c03376
ACS Nano 2020, 14, 12771−12780

mbar) with a room-temperature electromagnet setup, using a Keithley current source (with currents within the maximum range of ±20 μA for spin transport measurements) and a nanovoltmeter. Gate voltage was applied by a Keithley source meter.

ASSOCIATED CONTENT

Supporting Information

The Supporting Information is available free of charge at https://pubs.acs.org/doi/10.1021/acsnano.0c03376.

Raman spectrum of CVD graphene, uniformity of CVD graphene channels, surface charge transfer doping in graphene sheets and device doping, *IV* characteristics of spin injection and detection contacts, a summary of spin devices measured in this study, and gate dependence of contact resistance (PDF)

AUTHOR INFORMATION

Corresponding Author

M. Venkata Kamalakar − *Department of Physics and Astronomy, Uppsala University, SE-751 20 Uppsala, Sweden;* orcid.org/0000-0003-2385-9267; Email: venkata.mutta@physics.uu.se

Authors

J. Panda − *Department of Physics and Astronomy, Uppsala University, SE-751 20 Uppsala, Sweden*

M. Ramu − *Department of Materials Science and Engineering, Uppsala University, SE-751 03 Uppsala, Sweden*

Olof Karis − *Department of Physics and Astronomy, Uppsala University, SE-751 20 Uppsala, Sweden*

Tapati Sarkar − *Department of Materials Science and Engineering, Uppsala University, SE-751 03 Uppsala, Sweden;* orcid.org/0000-0003-4754-2504

Complete contact information is available at: https://pubs.acs.org/10.1021/acsnano.0c03376

Author Contributions

[§]J. Panda and M. Ramu are co-first authors.

Notes

The authors declare no competing financial interest.

ACKNOWLEDGMENTS

We gratefully acknowledge funding from Swedish Research Council (VR starting grants 2016-03278 and 2017-05030), Carl Tryggers Stiftelse för Vetenskaplig Forskning (grant no. CTS 18:271), Stiftelsen Olle Engkvist Byggmästare (200-0602), Energimyndigheten (48698-1), Formas (grant no. 2019-01326), and Wenner-Gren Stiftelserna (UPD2018-0057, UPD2018-0003, and UPD2019-0166). We thank Stephan Roche, Aron W. Cummings, and José M. Caridad for insightful discussions.

REFERENCES

(1) Tombros, N.; Jozsa, C.; Popinciuc, M.; Jonkman, H. T.; van Wees, B. J. Electronic Spin Transport and Spin Precession in Single Graphene Layers at Room Temperature. *Nature* **2007**, *448*, 571−574.

(2) Zomer, P. J.; Guimarães, M. H. D.; Tombros, N.; van Wees, B. J. Long-Distance Spin Transport in High-Mobility Graphene on Hexagonal Boron Nitride. *Phys. Rev. B: Condens. Matter Mater. Phys.* **2012**, *86*, 161416.

(3) Kamalakar, M. V.; Groenveld, C.; Dankert, A.; Dash, S. P. Long Distance Spin Communication in Chemical Vapour Deposited Graphene. *Nat. Commun.* **2015**, *6*, 6766.

(4) Dlubak, B.; Martin, M.-B.; Deranlot, C.; Servet, B.; Xavier, S.; Mattana, R.; Sprinkle, M.; Berger, C.; De Heer, W. A.; Petroff, F.; Anane, A.; Seneor, P.; Fert, A. Highly Efficient Spin Transport in Epitaxial Graphene on SiC. *Nat. Phys.* **2012**, *8*, 557−561.

(5) Huertas-Hernando, D.; Guinea, F.; Brataas, A. Spin-Orbit Coupling in Curved Graphene, Fullerenes, Nanotubes, and Nanotube Caps. *Phys. Rev. B: Condens. Matter Mater. Phys.* **2006**, *74*, 155426.

(6) Ingla-Aynés, J.; Guimarães, M. H. D.; Meijerink, R. J.; Zomer, P. J.; van Wees, B. J. 24−μm Spin Relaxation Length in Boron Nitride Encapsulated Bilayer Graphene. *Phys. Rev. B: Condens. Matter Mater. Phys.* **2015**, *92*, 201410.

(7) Serrano, I. G.; Panda, J.; Denoel, F.; Vallin, Ö.; Phuyal, D.; Karis, O.; Kamalakar, M. V. Two-Dimensional Flexible High Diffusive Spin Circuits. *Nano Lett.* **2019**, *19*, 666−673.

(8) Drögeler, M.; Franzen, C.; Volmer, F.; Pohlmann, T.; Banszerus, L.; Wolter, M.; Watanabe, K.; Taniguchi, T.; Stampfer, C.; Beschoten, B. Spin Lifetimes Exceeding 12 ns in Graphene Nonlocal Spin Valve Devices. *Nano Lett.* **2016**, *16*, 3533−3539.

(9) Drögeler, M.; Volmer, F.; Wolter, M.; Terrés, B.; Watanabe, K.; Taniguchi, T.; Güntherodt, G.; Stampfer, C.; Beschoten, B. Nanosecond Spin Lifetimes in Single- and Few-Layer Graphene-hBN Heterostructures at Room Temperature. *Nano Lett.* **2014**, *14*, 6050−6055.

(10) Avsar, A.; Yang, T.-Y.; Bae, S.; Balakrishnan, J.; Volmer, F.; Jaiswal, M.; Yi, Z.; Ali, S. R.; Güntherodt, G.; Hong, B. H.; Beschoten, B.; Özyilmaz, B. Towards Wafer Scale Fabrication of Graphene Based Spin Valve Devices. *Nano Lett.* **2011**, *11*, 2363−2368.

(11) Khokhriakov, D.; Karpiak, B.; Hoque, A. M.; Dash, S. P. Two-Dimensional Spintronic Circuit Architectures on Large Scale Graphene. *Carbon* **2020**, *161*, 892.

(12) Gebeyehu, Z. M.; Parui, S.; Sierra, J. F.; Timmermans, M.; Esplandiu, M. J.; Brems, S.; Huyghebaert, C.; Garello, K.; Costache, M. V.; Valenzuela, S. O. Spin Communication over 30 μm Long Channels of Chemical Vapor Deposited Graphene on SiO_2. *2D Mater.* **2019**, *6*, 034003.

(13) Verguts, K.; Defossez, Y.; Leonhardt, A.; De Messemaeker, J.; Schouteden, K.; Van Haesendonck, C.; Huyghebaert, C.; De Gendt, S.; Brems, S. Growth of Millimeter-Sized Graphene Single Crystals on Al_2O_3 (0001)/Pt(111) Template Wafers Using Chemical Vapor Deposition. *ECS J. Solid State Sci. Technol.* **2018**, *7*, M195−M200.

(14) Banszerus, L.; Schmitz, M.; Engels, S.; Goldsche, M.; Watanabe, K.; Taniguchi, T.; Beschoten, B.; Stampfer, C. Ballistic Transport Exceeding 28 μm in CVD Grown Graphene. *Nano Lett.* **2016**, *16*, 1387−1391.

(15) Mahmood, A.; Yang, C.-S. S.; Dayen, J.-F.; Park, S.; Kamalakar, M. V.; Metten, D.; Berciaud, S.; Lee, J. O.; Doudin, B. Room Temperature Dry Processing of Patterned CVD Graphene Devices. *Carbon* **2015**, *86*, 256−263.

(16) Hu, J.; Stecklein, G.; Deen, D. A.; Su, Q.; Crowell, P. A.; Koester, S. J. Scaling of the Nonlocal Spin and Baseline Resistances in Graphene Lateral Spin Valves. *IEEE Trans. Electron Devices* **2019**, *66*, 5003−5010.

(17) Cummings, A. W.; Dubois, S. M.-M.; Charlier, J.-C.; Roche, S. Universal Spin Diffusion Length in Polycrystalline Graphene. *Nano Lett.* **2019**, *19*, 7418−7426.

(18) Rashba, E. I. Theory of Electrical Spin Injection: Tunnel Contacts as a Solution of the Conductivity Mismatch Problem. *Phys. Rev. B: Condens. Matter Mater. Phys.* **2000**, *62*, R16267−R16270.

(19) Fert, A.; Jaffrès, H. Conditions for Efficient Spin Injection from a Ferromagnetic Metal into a Semiconductor. *Phys. Rev. B: Condens. Matter Mater. Phys.* **2001**, *64*, 184420.

(20) Giovannetti, G.; Khomyakov, P. A.; Brocks, G.; Karpan, V. M.; van den Brink, J.; Kelly, P. J. Doping Graphene with Metal Contacts. *Phys. Rev. Lett.* **2008**, *101*, 026803.

(21) Chaves, F. A.; Jiménez, D.; Cummings, A. W.; Roche, S. Physical Model of the Contact Resistivity of Metal-Graphene Junctions. *J. Appl. Phys.* **2014**, *115*, 164513.

(22) Nouchi, R.; Saito, T.; Tanigaki, K. Determination of Carrier Type Doped from Metal Contacts to Graphene by Channel-Length-

Dependent Shift of Charge Neutrality Points. *Appl. Phys. Express* **2011**, *4*, 035101.
(23) Thissen, N. F. W.; Vervuurt, R. H. J.; Mackus, A. J. M.; Mulders, J. J. L.; Weber, J.-W.; Kessels, W. M. M.; Bol, A. A. Graphene Devices with Bottom-up Contacts by Area-Selective Atomic Layer Deposition. *2D Mater.* **2017**, *4*, 025046.
(24) Mueller, T.; Xia, F.; Freitag, M.; Tsang, J.; Avouris, Ph. Role of Contacts in Graphene Transistors: A Scanning Photocurrent Study. *Phys. Rev. B: Condens. Matter Mater. Phys.* **2009**, *79*, 245430.
(25) Volmer, F.; Drögeler, M.; Güntherodt, G.; Stampfer, C.; Beschoten, B. Spin and Charge Transport in Graphene-Based Spin Transport Devices with Co/MgO Spin Injection and Spin Detection Electrodes. *Synth. Met.* **2015**, *210*, 42−55.
(26) Sosenko, E.; Wei, H.; Aji, V. Effect of Contacts on Spin Lifetime Measurements in Graphene. *Phys. Rev. B: Condens. Matter Mater. Phys.* **2014**, *89*, 245436.
(27) Guimarães, M. H. D.; Veligura, A.; Zomer, P. J.; Maassen, T.; Vera-Marun, I. J.; Tombros, N.; van Wees, B. J. Spin Transport in High-Quality Suspended Graphene Devices. *Nano Lett.* **2012**, *12*, 3512−3517.
(28) Maassen, T.; Vera-Marun, I. J.; Guimarães, M. H. D.; van Wees, B. J. Contact-Induced Spin Relaxation in Hanle Spin Precession Measurements. *Phys. Rev. B: Condens. Matter Mater. Phys.* **2012**, *86*, 235408.
(29) Gurram, M.; Omar, S.; Zihlmann, S.; Makk, P.; Schönenberger, C.; Van Wees, B. J. Spin Transport in Fully Hexagonal Boron Nitride Encapsulated Graphene. *Phys. Rev. B: Condens. Matter Mater. Phys.* **2016**, *93*, 115441.
(30) Vila, M.; Garcia, J. H.; Cummings, A. W.; Power, S. R.; Groth, C. W.; Waintal, X.; Roche, S. Nonlocal Spin Dynamics in the Crossover from Diffusive to Ballistic Transport. *Phys. Rev. Lett.* **2020**, *124*, 196602.
(31) Huang, P. Y.; Ruiz-Vargas, C. S.; van der Zande, A. M.; Whitney, W. S.; Levendorf, M. P.; Kevek, J. W.; Garg, S.; Alden, J. S.; Hustedt, C. J.; Zhu, Y.; Park, J.; McEuen, P. L.; Muller, D. A. Grains and Grain Boundaries in Single-Layer Graphene Atomic Patchwork Quilts. *Nature* **2011**, *469*, 389−392.
(32) Kim, K.; Lee, Z.; Regan, W.; Kisielowski, C.; Crommie, M. F.; Zettl, A. Grain Boundary Mapping in Polycrystalline Graphene. *ACS Nano* **2011**, *5*, 2142−2146.
(33) Fan, X.; Wagner, S.; Schädlich, P.; Speck, F.; Kataria, S.; Haraldsson, T.; Seyller, T.; Lemme, M. C.; Niklaus, F. Direct Observation of Grain Boundaries in Graphene through Vapor Hydrofluoric Acid (VHF) Exposure. *Sci. Adv.* **2018**, *4*, 1−10.
(34) Ochoa, H.; Castro Neto, A. H.; Guinea, F. Elliot-Yafet Mechanism in Graphene. *Phys. Rev. Lett.* **2012**, *108*, 206808.
(35) Zhang, P.; Wu, M. W. Electron Spin Relaxation in Graphene with Random Rashba Field: Comparison of the D'yakonov−Perel' and Elliott−Yafet-like Mechanisms. *New J. Phys.* **2012**, *14*, 033015.
(36) Huertas-Hernando, D.; Guinea, F.; Brataas, A. Spin-Orbit-Mediated Spin Relaxation in Graphene. *Phys. Rev. Lett.* **2009**, *103*, 146801.
(37) Han, W.; Kawakami, R. K. Spin Relaxation in Single-Layer and Bilayer Graphene. *Phys. Rev. Lett.* **2011**, *107*, 047207.
(38) Stecklein, G.; Crowell, P. A.; Li, J.; Anugrah, Y.; Su, Q.; Koester, S. J. Contact-Induced Spin Relaxation in Graphene Nonlocal Spin Valves. *Phys. Rev. Appl.* **2016**, *6*, 054015.
(39) Fratini, S.; Gosálbez-Martínez, D.; Merodio Cámara, P.; Fernández-Rossier, J. Anisotropic Intrinsic Spin Relaxation in Graphene Due to Flexural Distortions. *Phys. Rev. B: Condens. Matter Mater. Phys.* **2013**, *88*, 115426.
(40) Huertas-Hernando, D.; Guinea, F.; Brataas, A. Spin Relaxation Times in Disordered Graphene. *Eur. Phys. J.: Spec. Top.* **2007**, *148*, 177−181.
(41) Van Tuan, D.; Ortmann, F.; Soriano, D.; Valenzuela, S. O.; Roche, S. Pseudospin-Driven Spin Relaxation Mechanism in Graphene. *Nat. Phys.* **2014**, *10*, 857−863.
(42) Cummings, A. W.; Roche, S. Effects of Dephasing on Spin Lifetime in Ballistic Spin-Orbit Materials. *Phys. Rev. Lett.* **2016**, *116*, 086602.
(43) Kochan, D.; Gmitra, M.; Fabian, J. Spin Relaxation Mechanism in Graphene: Resonant Scattering by Magnetic Impurities. *Phys. Rev. Lett.* **2014**, *112*, 116602.
(44) Lundeberg, M. B.; Yang, R.; Renard, J.; Folk, J. A. Defect-Mediated Spin Relaxation and Dephasing in Graphene. *Phys. Rev. Lett.* **2013**, *110*, 156601.
(45) Foa Torres, L. E. F.; Roche, S.; Charlier, J.-C. *Introduction to Graphene-Based Nanomaterials*; Cambridge University Press, 2020; DOI: 10.1017/9781108664462.
(46) Whelan, P. R.; Shen, Q.; Zhou, B.; Serrano, I. G.; Kamalakar, M. V.; MacKenzie, D. M. A.; Ji, J.; Huang, D.; Shi, H.; Luo, D.; Wang, M.; Ruoff, R. S.; Jauho, A.-P.; Jepsen, P. U.; Bøggild, P.; Caridad, J. M. Fermi Velocity Renormalization in Graphene Probed by Terahertz Time-Domain Spectroscopy. *2D Mater.* **2020**, *7*, 035009.
(47) Amamou, W.; Lin, Z.; van Baren, J.; Turkyilmaz, S.; Shi, J.; Kawakami, R. K. Contact Induced Spin Relaxation in Graphene Spin Valves with Al_2O_3 and MgO Tunnel Barriers. *APL Mater.* **2016**, *4*, 032503.
(48) Muscas, G.; Jönsson, P. E.; Serrano, I. G.; Vallin, Ö.; Kamalakar, M. V. Flexible Ferromagnetic Nanowires with Ultralow Magnetostriction. *arXiv*, 2006.10687v1, https://arxiv.org/abs/2006.10687.
(49) Kamalakar, M. V.; Dankert, A.; Bergsten, J.; Ive, T.; Dash, S. P. Enhanced Tunnel Spin Injection into Graphene Using Chemical Vapor Deposited Hexagonal Boron Nitride. *Sci. Rep.* **2014**, *4*, 6146.
(50) Kamalakar, M. V.; Dankert, A.; Kelly, P. J.; Dash, S. P. Inversion of Spin Signal and Spin Filtering in Ferromagnet|Hexagonal Boron Nitride-Graphene van der Waals Heterostructures. *Sci. Rep.* **2016**, *6*, 21168.
(51) Dayen, J.-F.; Ray, S. J.; Karis, O.; Vera-Marun, I. J.; Kamalakar, M. V. Two-Dimensional van der Waals Spinterfaces and Magnetic-Interfaces. *Appl. Phys. Rev.* **2020**, *7*, 011303.
(52) Avsar, A.; Ochoa, H.; Guinea, F.; Özyilmaz, B.; van Wees, B. J.; Vera-Marun, I. J. Colloquium: Spintronics in Graphene and Other Two-Dimensional Materials. *Rev. Mod. Phys.* **2020**, *92*, 021003.
(53) McCreary, K. M.; Hanbicki, A. T.; Robinson, J. T.; Cobas, E.; Culbertson, J. C.; Friedman, A. L.; Jernigan, G. G.; Jonker, B. T. Large-Area Synthesis of Continuous and Uniform MoS_2 Monolayer Films on Graphene. *Adv. Funct. Mater.* **2014**, *24*, 6449−6454.
(54) Serrano, I. G.; Panda, J.; Edvinsson, T.; Kamalakar, M. V. Flexible Transparent Graphene Laminates *Via* Direct Lamination of Graphene onto Polyethylene Naphthalate Substrates. *Nanoscale Adv.* **2020**, *2*, 3156−3163.

https://dx.doi.org/10.1021/acsnano.0c03376
ACS Nano 2020, 14, 12771−12780